J Appl Electrochem (2008) 38:207–214
DOI 10.1007/s10800-007-9426-x

ORIGINAL PAPER

Comparison of the corrosion behaviour in 5% NaCl solution of Mg alloys NZ30K and AZ91D

J. W. Chang · L. M. Peng · X. W. Guo · A. Atrens · P. H. Fu · W. J. Ding · X. S. Wang

Received: 4 April 2007 / Revised: 21 September 2007 / Accepted: 21 September 2007 / Published online: 5 October 2007

Abstract The corrosion behaviour of AZ91D and NZ30K (Mg–3Nd–0.2Zn–0.4Zr) alloys was investigated in 5% NaCl solution by immersion tests and electrochemical measurements. The immersion tests showed that the corrosion rate of NZ30K was about half that of AZ91D. The localized corrosion of AZ91D was more severe than that of NZ30K due to the higher cathode-to-anode area ratio and higher difference in potential of the cathode phase and the anode matrix. The corrosion of AZ91D concentrated on certain areas and resulted in much deeper corrosion pits, whilst that of NZ30K spread across the surface and led to more uniform and shallow corroded areas. The corrosion products of NZ30K were more compact than those of AZ91D as indicated by SEM. The cyclic polarization curves showed that NZ30K had higher pitting corrosion resistance than AZ91D.

J. W. Chang (✉) · L. M. Peng · X. W. Guo · P. H. Fu · W. J. Ding
National Engineering Research Center of Light Alloys Net Forming (LAF), School of Materials Science and Engineering, Shanghai Jiaotong University, 1954 Huashan Road, Shanghai 200030, China
e-mail: changjw@sjtu.edu.cn

A. Atrens
Materials Engineering, The University of Queensland, Brisbane 4072, Australia

A. Atrens
Swiss Federal Laboratories for Materials Science and Technology, EMPA, Dept. 136, Überlandstrasse 129, 8600 Dubendorf, Switzerland

X. S. Wang
School of Aerospace, Tsinghua University, Beijing 100084, China

Keywords AZ91D · Corrosion behaviour · Cyclic polarization · Mg–Nd–Zn–Zr alloy

1 Introduction

Magnesium alloys are light structural and functional materials used in the automotive, aerospace, electronic, and energy industries. However, the low corrosion resistance of magnesium alloys limits their applications. To extend current applications, much work on the corrosion mechanisms of magnesium alloys have been carried out during the past decade [1–10]. Most of these investigations have focused on the most popular Mg alloys based on the Mg–Al system, such as AZ91 and AM50. Although it is well known that rare earth additions improve the mechanical properties [11–14], there is relatively little research into the influence of rare earth elements on the corrosion behaviour of the magnesium alloys [15–16]. Generally, rare earth elements improve corrosion resistance [17, 18]. Recently, Chang et al. [19] reported that the corrosion rate of Mg–3Nd–0.2Zn–0.4Zr (NZ30K) in 5% NaCl solution was only half that of AZ91D, which is believed to have good corrosion resistance. However, the reason for the different corrosion rates for AZ91D and NZ30K has not been investigated. The present paper studies the corrosion and electrochemical behaviour of NZ30K and AZ91D alloys in 5% NaCl solution.

2 Experimental

The commercial AZ91D magnesium alloy had a nominal composition as Al 9%, Zn 1% and Mg balance. NZ30K had the composition as Nd 3%, Zn 0.2%, Zr 0.4% and Mg

balance [19]. Specimens were cut from as-cast ingots. Scanning electron microscopy (SEM) was used to characterize the microstructures, the morphologies of the corrosion products after the immersion test and the corroded surfaces after removal of the corrosion products. The cross section of each corroded specimen was characterized using optical microscopy (OM). Depth profiles through the corrosion products were characterized using Auger electron spectroscopy (AES) combined with Ar ion etching. Quantitative determination of the composition was based on the literature values of the sensitivity factors [20] and was carried out using the general survey spectra.

Specimens for immersion test were cut into coupons, 5 mm thickness and 30 mm in diameter, ground with 320 grit Al_2O_3 waterproof abrasive paper and 3 grit metallographic paper, washed with distilled water, degreased with alcohol and immediately immersed in the 5% NaCl solution. The specimens were suspended in the solution by means of a Nylon string through a hole, 0.25 mm in diameter, drilled near one edge. The immersion test consisted of 3 days continuous immersion at 25 ± 2 °C with no stirring. The solution pH increased from neutral to about 11 within a few hours, and remained stable at that value during the remainder of the test. Therefore, it was not necessary to saturate the solution with $Mg(OH)_2$. The corrosion products were removed by immersion in a 200 g/L chromate acid solution with 10 g/L silver nitrate at room temperature for 7 min, and the weight loss was determined.

For electrochemical measurements, the 5% NaCl solution was saturated with $Mg(OH)_2$ to give a stable pH of around 11. Open circuit potential measurements began immediately after the specimens were immersed in the solution. A cyclic polarization scan was started from a cathodic potential at a rate of 1 mV/s. After the potential reached a set anodic potential, the scan was reversed. Electrochemical measurements were performed with Advanced Electrochemical System PARSTAT 2273 from Princeton Applied Research. The apparatus were described elsewhere [21].

3 Results and discussion

3.1 Microstructure

Figure 1a presents the microstructure of AZ91D. The microstructure consisted of primary α, the eutectic micro-constituent and the β phase (marked in Fig. 1a). The β phase was the intermetallic compound $Mg_{17}Al_{12}$. The eutectic micro-constituent consisted of lamellae of the α-phase and the β phase next to large β phase particles.

In fast cooled ingot of AZ91, the microstructure consisted of the primary α and a divorced eutectic micro-constituent consisting of β phase and secondary α [22].

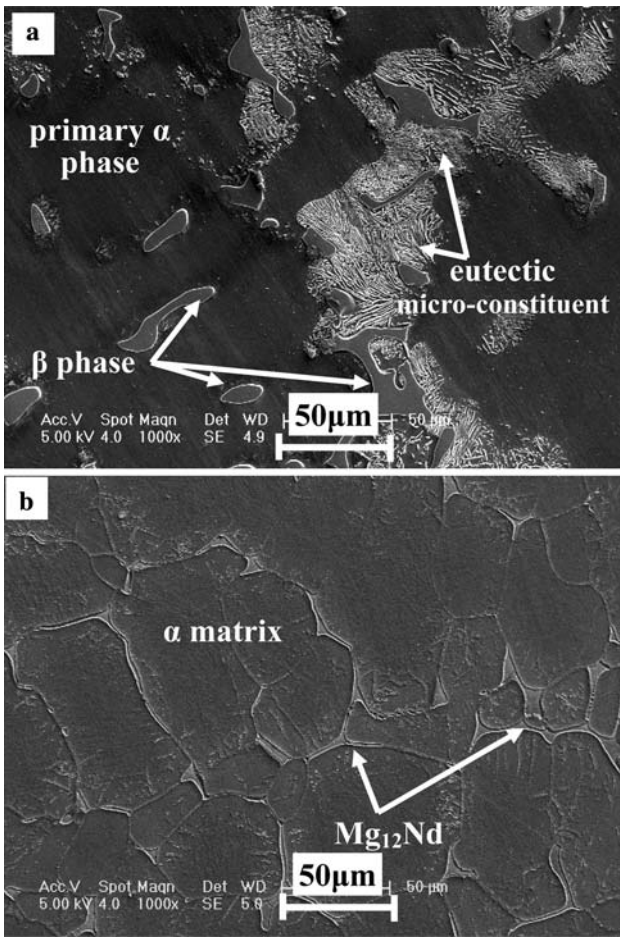

Fig. 1 SEM micrographs of two alloys: (**a**) AZ91D, (**b**) NZ30K

Under these conditions the primary α had a much lower Al content than the secondary α. The ingot used in this study however appeared to have been relatively slowly cooled so that the eutectic micro-constituent was the lamellae arrangement of the α-phase and the β phase. Under these conditions it could be that the primary α had similar Al content to that of the secondary α.

The microstructure of NZ30K alloy, as shown in Fig. 1b, was composed of the α magnesium matrix and the eutectic compound $Mg_{12}Nd$ distributed along the α dendrite boundaries. EDX analysis, not presented here, showed that the zinc had partitioned in $Mg_{12}Nd$ phase, the concentration of zinc in the α matrix was negligible. Zr was added to refine the grain size of NZ30K alloy. The distribution of the second phase ($Mg_{17}Al_{12}$ in AZ91D and $Mg_{12}Nd$ in NZ30K) was not continuous for either alloy.

3.2 Corrosion of AZ91D and NZ30K

Table 1 presents the corrosion rates for AZ91D and NZ30K immersed in 5% NaCl solution for 3 days. NZ30K

was more corrosion resistant than AZ91D as the corrosion rate of NZ30K was about half that of AZ91D. Figure 2 shows that both alloys evinced localized corrosion although the extent of corrosion was different. The area of localized corrosion on NZ30K was much larger than that on AZ91D. However, AZ91D had many deep pits, whilst the depth of the corroded areas was relatively shallow for NZ30K.

Figure 3 shows the morphologies of the corroded surface of AZ91D and NZ30K after immersion in 5% NaCl solution for 3 days and removal of the corrosion products. The corrosion pit of AZ91D was much deeper than that of NZ30K. The corrosion of NZ30K had spread from one grain to another across the surface, whilst the corrosion of AZ91D had extended along the longitudinal direction and resulted in much deeper corrosion pits. Optical micrographs of the cross sections through the corroded surface after the immersion test and removal of the corrosion products (Fig. 4) indicated that corrosion had attacked the matrix preferentially, and the second phase ($Mg_{17}Al_{12}$ in AZ91D and $Mg_{12}Nd$ in NZ30K) was not corroded. The corrosion of the α matrix near the $Mg_{12}Nd$ phase in NZ30K (Fig. 4b) was less severe than that of α matrix near the $Mg_{17}Al_{12}$ phase in AZ91D (Fig. 4a). This indicates that the galvanic corrosion between the $Mg_{12}Nd$ phase and the α matrix in NZ30K was less severe than that between the $Mg_{17}Al_{12}$ phase and the α phase in AZ91D.

3.3 Effect of microstructure on corrosion behaviour

The difference in corrosion rate of AZ91D and NZ30K was related to the microstructure. Figure 1 shows that the microstructure of AZ91D was composed of the primary α, the eutectic micro-constituent and β phase, whilst that of NZ30K consisted of $Mg_{12}Nd$ and the α matrix. The second phase in a magnesium alloy was often inert and stable. Figure 4 shows that the $Mg_{17}Al_{12}$ phase in AZ91D and $Mg_{12}Nd$ in NZ30K were still intact in the corroded areas. Earlier investigations on the corrosion behaviour of AZ91 alloy have shown that the β phase can play a dual role in the corrosion behaviour [5, 6]. It could act as either a galvanic cathode or a barrier to corrosion. Which role dominated the corrosion process depended on the amount and distribution of the β phase. Finely and continuously distributed β phase could more effectively stop the corrosion. The higher

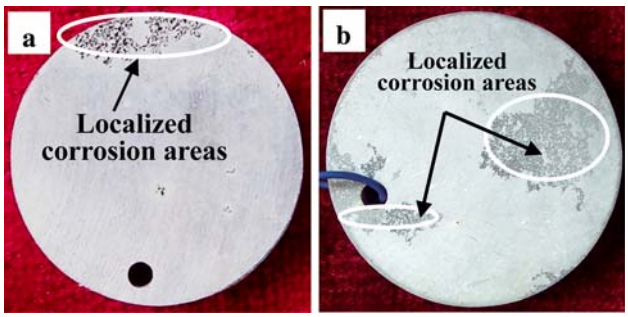

Fig. 2 Corroded surfaces after immersion in 5% NaCl solution for 3 days and removal of the corrosion products. (**a**) AZ91D, (**b**) NZ30K

corrosion resistance of die cast AZ91 compared with gravity cast alloy was due to the higher volume fraction and more continuous distribution of the β phase along the grain boundaries, which acted as an effective corrosion barrier [22]. Otherwise, if the fraction of the β phase was low and the distribution was not continuous, the β phase accelerated corrosion. The $Mg_{12}Nd$ phase in NZ30K had a similar role as the β phase in AZ91D. As shown in Fig. 4, the β phase in AZ91D and $Mg_{12}Nd$ in NZ30K could not act as effective corrosion barrier, and both can form galvanic coupling with the α matrix. This was because of the small amount of β phase in AZ91D and $Mg_{12}Nd$ in NZ30K and its discontinuous distribution (Fig. 1). Because the Al content of AZ91D can be heterogeneously distributed, there have been many investigations on the influence of Al distribution on the corrosion behaviour [10, 22–24]. Many studies have found that the corrosion rate decreases with increasing Al content. Ambat et al. [10] found that the preferentially corroded region was the α matrix with an Al concentration less than 8%. In NZ30K, zirconium was a powerful grain refiner and also an effective purifier. Zirconium can react with iron or nickel in the molten magnesium to form insoluble precipitates which settle to the bottom of the molten magnesium because of their higher density. The zirconium in NZ30K can lead to high purity and hence more corrosion resistance. The effect of Zr on corrosion behaviour of Mg–RE alloy was discussed previously [15]. The small amount of zinc (0.2% in NZ30K) had little effect on the corrosion behaviour of as-cast NZ30K. A more detailed investigation will be reported later.

The predominant factors determining the rate of micro-galvanic corrosion included the cathode-to-anode area ratio and the difference in potentials of the two phases [25].

Table 1 Corrosion rates of AZ91D and NZ30K in 5% NaCl solution for 3 days

Alloy	Corrosion rate-1 (mg cm^{-2} day^{-1})	Corrosion rate-2 (mg cm^{-2} day^{-1})	Corrosion rate-3 (mg cm^{-2} day^{-1})	Average corrosion rate (mg cm^{-2} day^{-1})
AZ91D	0.463	0.403	0.552	0.473
NZ30K	0.217	0.202	0.205	0.208

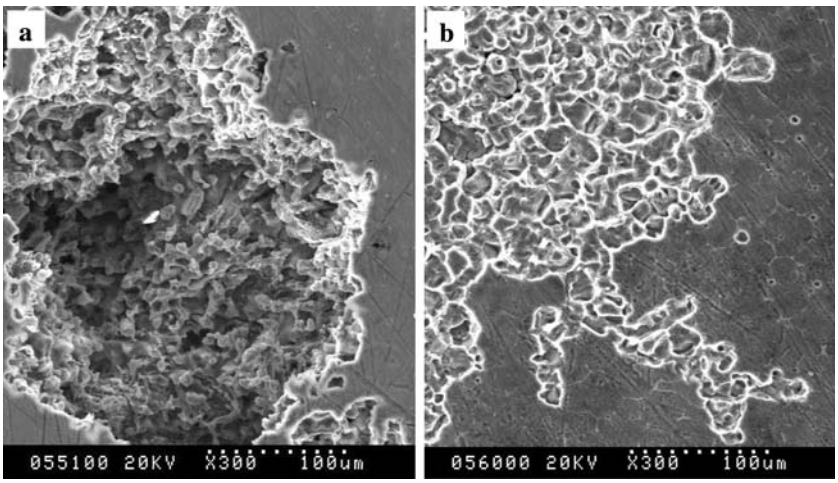

Fig. 3 SEM micrographs of the corroded surfaces after immersion in 5% NaCl solutions for 3 days and removal of the corrosion products. (**a**) AZ91D, (**b**) NZ30K

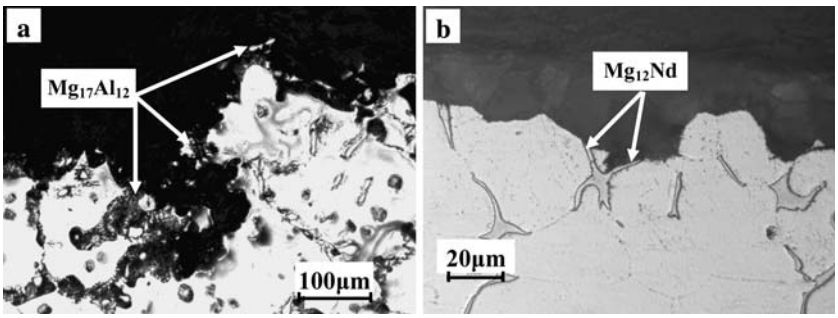

Fig. 4 Typical optical micrographs through the corroded surfaces after immersion in 5% NaCl solutions for 3 days and removal of the corrosion products. (**a**) AZ91D, (**b**) NZ30K

Galvanic corrosion can be accelerated when the cathode-to-anode area ratio is greater than 0.5. The solubility of Nd in magnesium is lower than that of Al. Figure 1 indicates that the volume fraction of $Mg_{12}Nd$ in NZ30K was lower than that of $Mg_{17}Al_{12}$ in AZ91D. This resulted in the greater cathode-to-anode area ratio for AZ91D than that for NZ30K. Song et al. [4], by studying specimens of the composition of the individual phases, showed that in 1 M NaCl solution, the potential of the β phase (–1.3 V/SCE) was some 300 mV positive to the α phase (–1.6 V/SCE). Skar et al. [26] attributed the higher corrosion resistance of Mg–RE alloys to the formation of less cathodic intermetallic compounds than $Mg_{17}Al_{12}$ in AZ alloy. Therefore, based on the principles of cathode-to-anode area ratio and the difference in potential of the two phases in galvanic corrosion, it seems likely that the β phase in AZ91D can cause more significant galvanic corrosion than $Mg_{12}Nd$ in NZ30K. This explains why the localized corrosion in AZ91D was more severe than that in NZ30K (Figs. 3 and 4) and that the corrosion rate of NZ30K was lower than that of AZ91D (Table 1).

3.4 Corrosion products

The morphologies of the corrosion products of AZ91D and NZ30K alloys after immersion in 5% NaCl solution for 3 days are compared in Fig. 5. The corrosion product of AZ91D was composed of voluminous tiny erect flakes and was similar to a honeycomb. The flakes were aligned perpendicular to the alloy surface. In contrast, the corrosion product of NZ30K consisted of many platelet-like flakes, which were not perpendicular to the alloy surface and formed a corrosion product film more compact than that of AZ91D.

The AES depth profiles of the corrosion product film formed on AZ91D after immersion in 5% NaCl solution for 120 min are presented in Fig. 6. Nordien et al. [27] showed that the corrosion film of AZ alloys presented a three-layered structure. As a result, three layers were marked with the dashed vertical lines in Fig. 6. Figure 6a shows that the Mg and O concentrations in the intermediate layer were slightly lower than that in the outer layer. In the inner layer, the Mg concentration increased gradually to the concentration in the substrate, and the oxygen concentration decreased to zero. Figure 6b shows that the Al and Zn contents increased with depth in the corrosion film except for a slight fluctuation in the outer layer. The inner layer was more enriched with Al and Zn than the outer layer. According to the previous studies [27, 28], the higher Al content in the inner layer resulted in increased stability of the corrosion product film and consequently improved corrosion resistance of the alloy. The zinc in the inner layer

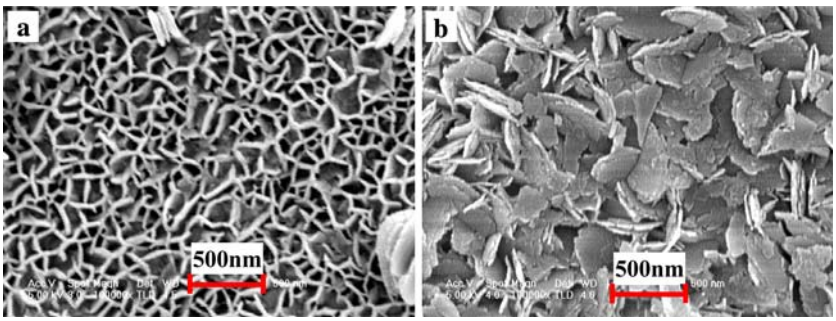

Fig. 5 SEM micrographs of the corrosion products after immersion in 5% NaCl solutions for 3 days. (**a**) AZ91D, (**b**) NZ30K

also improved the passive properties of the corrosion film by reducing the degree of hydration [27].

Figure 7 shows AES depth profiles for the corrosion film on NZ30K, which was immersed in 5% NaCl solution for 30 min. A transition existed between the corrosion product film and the substrate in Fig. 7a. The Mg and O concentrations were nearly uniform in the corrosion product film. In the transition layer, the Mg content increased and the O content decreased. The Nd, Zn and Zr contents in the transition were much higher than that in the corrosion product film, in which the Nd, Zn and Zr contents were nearly uniform (Fig. 7b). The presence of the rare earth elements in the corrosion product film has been thought to increase the corrosion resistance of the alloy [29]. Miller et al. [30] attributed the good corrosion resistance of non-equilibrium Mg–Y alloys to the enrichment of oxidized Y in the corrosion product films in alkaline solution containing chloride ions. Krishnamurthy et al. [31] noted a pseudo-passivation behaviour in rapidly solidified binary Mg-10–26%Nd alloy; the pseudo-passivation was attributed to Nd enrichment in the corrosion product film. Nordien et al. [27] found that the presence of RE elements caused a significant reduction in film hydration and improved the passive properties of the corrosion film. Yao et al. [32] suggested that the corrosion was inhibited due to the trapping of anions (such as Cl^- and CO_3^{2-}) in the corrosion products by RE elements. The increase of Zr content in the transition layer was attributed to its lower activity than Mg.

Figures 6a and 7a show that the corrosion product film on the NZ30K alloy was much thicker than that on AZ91D: the sputtering time of NZ30K was about four times longer than that of AZ91D. This indicated that the corrosion product film of NZ30K grew faster than that of AZ91D, which appeared to be contradictory to the results of the immersion test (Table 1) that the corrosion rate of AZ91D was higher than that of NZ30K. This was attributed to the different immersion time for the AES measurements and the immersion tests. For AES characterization, the corrosion films were formed after short immersion time (120 min for AZ91D and 30 min for NZ30K), whereas in the immersion test, the corrosion rates were measured during a longer immersion time (3 days). In the initial immersion time, general corrosion occurred on NZ30K and AZ91D, and the corrosion rate of NZ30K was higher than that of AZ91D. For long immersion times localized corrosion occurred on AZ91D and NZ30K and the galvanic corrosion of AZ91D was much more severe than that for NZ30K. Therefore AZ91D had a higher corrosion rate than NZ30K in the immersion tests.

3.5 Open circuit potential

The open circuit potential (E_{OC}) experiments were carried out in 5% NaCl solution saturated with $Mg(OH)_2$ and the results are presented in Fig. 8. The corrosion potential of AZ91D increased quickly during the initial period of about

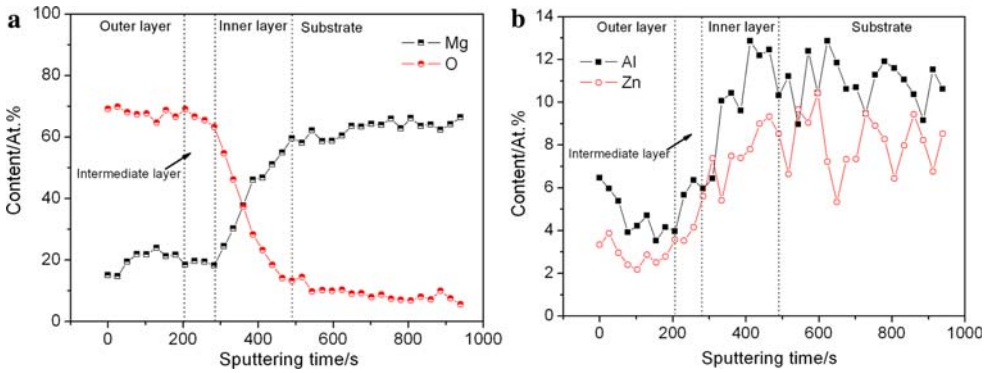

Fig. 6 AES depth profiles of the corrosion film formed on AZ91D after immersion in 5% NaCl solution for 120 min: (**a**) Mg and O, (**b**) Al and Zn

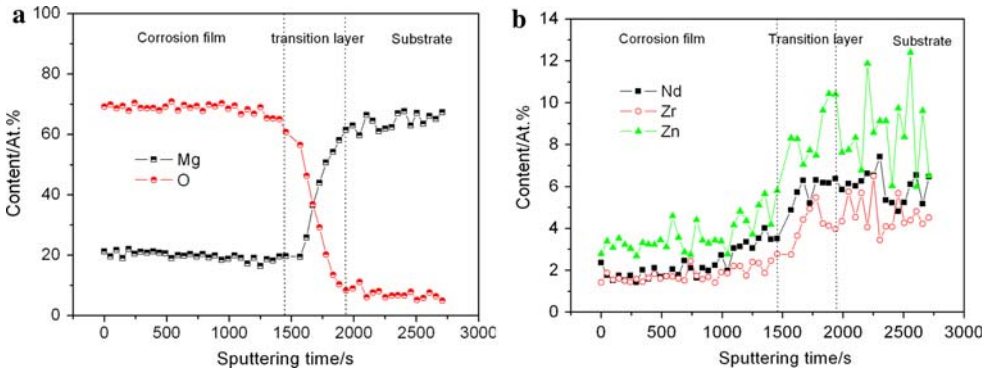

Fig. 7 AES depth profiles of the corrosion film formed on NZ30K after immersion in 5% NaCl solution for 30 min: (**a**) Mg and O, (**b**) Nd, Zn and Zr

10 min and then decreased rapidly until some pits were formed (after about 20 min) and hydrogen bubbles were evolved from the pits. In contrast, the corrosion potential of NZ30K increased slowly until it reached around –1.65V/SCE after immersion for about 7 h. At that time, the corrosion potential of NZ30K decreased suddenly due to the initiation of localized corrosion. Hydrogen bubbles evolved from the corrosion pits. After 7 h of immersion, the pits spread across the surface of the electrode. During the exposure time tested AZ91D showed a more positive corrosion potential than NZ30K. Nakatsugawa et al. [33] also found that the corrosion potentials of Mg–RE alloys (Mg–Gd, Mg–Dy, Mg–Nd–Zr, Mg–Gd–Nd–Zr and Mg–Dy–Nd–Zr) were more negative than that of AZ91D in 5% NaCl solution saturated with $Mg(OH)_2$.

3.6 Cyclic polarization

Figures 2 and 3 show that both AZ91D and NZ30K suffered localized corrosion during the immersion test. A cyclic polarization curve can indicate the tendency of a material to undergo pitting in a specific corrosion environment. The technique was particularly useful in the development of alloys with high pitting resistance. Figure 9 presents cyclic polarization curves for AZ91D and NZ30K after immersion in 5% NaCl solution saturated with $Mg(OH)_2$ for 1 h. On the forward scans the corrosion potential of AZ91D at –1.52 V was less active than that of NZ30K at –1.75 V. On the reverse scans the corrosion potential of AZ91D was –1.73 V and that of NZ30K was –1.72 V. The corrosion potential of the reverse scan for AZ91D shifted to a more negative value than on the forward scan, whilst that for NZ30K was more positive than that of the forward scan. The difference for NZ30K of 0.03 V was much smaller than 0.21 V for AZ91D.

Generally, the cathodic polarization curves were assumed to represent the cathodic hydrogen evolution, whilst the anodic curves represented the dissolution of magnesium. The cathodic parts of the forward scan curves in Fig. 9 show that the cathodic polarization current on NZ30K was much lower than that on AZ91D (or NZ30K shows a higher hydrogen overpotential than AZ91D). This indicated that the hydrogen evolution reaction was easier on AZ91D than on NZ30K. The anodic part of the forward

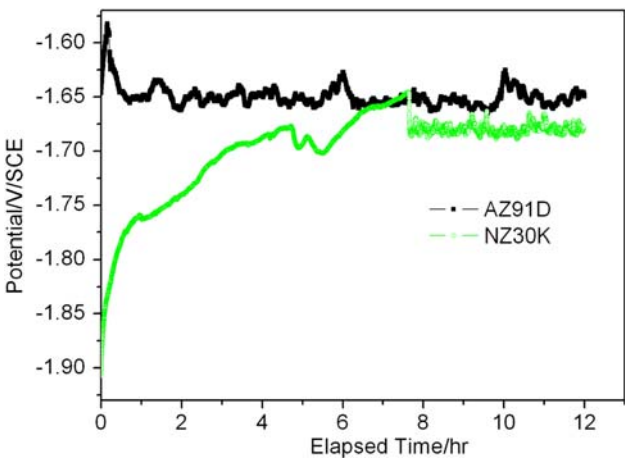

Fig. 8 Variation of E_{OC} of AZ91D and NZ30K after immersion in 5% NaCl solution saturated with $Mg(OH)_2$

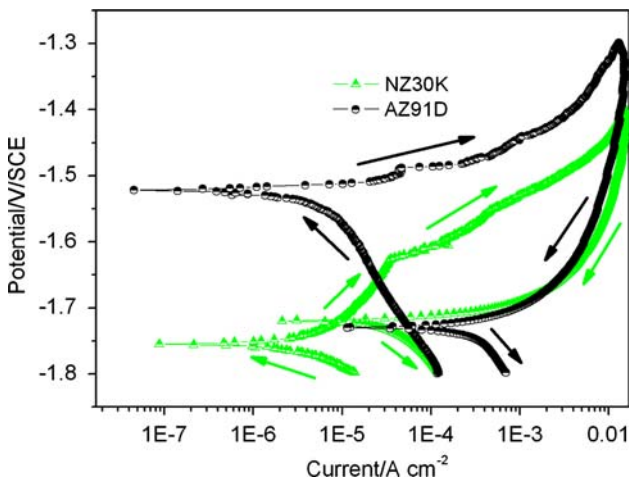

Fig. 9 Cyclic polarization curves of AZ91D and NZ30K after immersion in 5% NaCl solution saturated with $Mg(OH)_2$ for 1 h

scan curve for NZ30K in Fig. 9 revealed a knee point (–1.63 V). Before the knee point, the current density increased slowly with increasing potential. After the knee point, the current density increased rapidly. In contrast, there was no distinct knee point on the anodic curve of AZ91D and the current density increased quickly after the electrode potential exceeded the corrosion potential. This was attributed to the lower compactness of corrosion product film on AZ91D than that on NZ30K (Fig. 5). According to the study of Hara et al. [34], the corrosion product films formed on Mg alloys during open-circuit immersion were protective and led to spontaneous passivation. When the electrode potential exceeded a critical value (pitting potential), the current density began to increase sharply. This increase in current density was followed by the evolution of hydrogen on the electrode surface, and the corrosion film suffered local breakdown. Figure 9 indicates that, for AZ91D alloy, the corrosion potential and the pitting potential were almost superimposed and the alloy corroded with pit formation at the corrosion potential. In contrast NZ30K was still in a "pseudo" passive state at the corrosion potential, and localized corrosion only occurred after the electrode potential increased to –1.63 V, which was much higher than the corrosion potential (–1.75 V). This also corroborated the fact that the corrosion behaviour of the two alloys was different. The anodic parts of the forward scans in Fig. 9 also show that the anodic current density of NZ30K was much higher than that of AZ91D. Song and StJohn [15] suggested that the difference in anodic currents was due to the difference in the cathodic hydrogen evolution rates from the uncorroded surfaces. Once the corrosion film suffered breakdown, the difference between the anodic should not be significant. That was why the anodic curves of NZ30K and AZ91D were similar in the reverse scan (Fig. 9).

The forward scan, particularly before the knee point, to some degree represented the polarization behaviour of the non-corroded areas whilst the reverse scan was associated with the corroded areas. Due to the galvanic effect, an area with a more negative potential was corroded and the area with a more positive potential was protected. For AZ91D the corrosion potential of the forward curve was higher than that of the reverse curve. This means the corrosion in a corroded area on AZ91D was accelerated by the non-corroded surrounding area and the surrounding area was protected by the corrosion in the corroded area. Consequently, the corrosion of AZ91D extended along the longitudinal direction and resulted in much deeper corrosion pits. In contrast, for NZ30K, the corrosion potential of the forward curve was lower than that of the reverse curve. This means the corrosion in the corroded area on NZ30K was likely to be retarded by the non-corroded surrounding area and the non-corroded area was easily attacked by the corrosion occurring next to it. As a result, the corrosion of NZ30K spread across the surface from grain to grain and resulted in shallow and uniform corroded areas. This also provided an explanation from an electrochemical point of view of the different corrosion morphologies of AZ91D and NZ30K (Figs. 2 and 3).

4 Conclusions

(1) NZ30K had higher corrosion resistance than AZ91D. The corrosion rate of NZ30K was only half that of AZ91D in 5% NaCl solution. Owing to the higher cathode-to-anode area ratio and higher difference in potential of the cathode phase and anode matrix, the localized corrosion on AZ91D was more severe than that of NZ30K. The corrosion of NZ30K spread across the surface, whilst that of AZ91D extend along the longitudinal direction and resulted in much deeper corrosion pits in certain areas.

(2) NZ30K and AZ91D had different corrosion product morphologies. The corrosion product film of NZ30K was more compact than that of AZ91D.

(3) Open circuit potential measurements indicated that the corrosion potential of AZ91D was higher than that of NZ30K. The cyclic polarization scans show that NZ30K had higher pitting corrosion resistance than AZ91D.

Acknowledgements This work was supported in part by the National Natural Science Foundation of China (50571047 and 5133003C). The authors thank Dr. Zheng-Ming Ding and Dr. Yi-Jian Lai of the Center of Analysis and Measurement of Shanghai Jiao Tong University for their assistance with the Field Emission Scanning Electron Microscopy (FE-SEM).

References

1. Li Y, Zhang T, Wang FH (2006) Electrochim Acta 51:2845
2. Ballerini G, Bardi U, Bignucolo R, Ceraolo G (2005) Corros Sci 47:2173
3. Mathieu S, Rapin C, Steinmetz J, Steinmetz P (2003) Corros Sci 45:2741
4. Song G, Atrens A, Wu X, Zhang B (1998) Corros Sci 40:1769
5. Song G, Atrens A (1999) Adv Eng Mater 1:11
6. Song G, Atrens A (2003) Adv Eng Mater 5:837
7. Song G (2005) Adv Eng Mater 7:563
8. Baril G, Blanc C, Pebere N (2001) J Electrochem Soc 148:B489
9. Lafront AM, Zhang W, Jin S, Tremblay R, Dube D, Ghali E (2005) Electrochem Acta 51:489
10. Ambat R, Aung NN, Zhou W (2000) Corros Sci 42:1433
11. Vostry P, Stulikova I, Smola B, Cieslar M, Mordike B (1988) Z Metall 79(5):340
12. Mei LY, Dunlop GL, Westengen H (1996) J Mater Sci 31:387
13. Rokhlin LL (2003) Magnesium alloys containing rare earth metals. Taylor & Francis, London

14. Rokhlin LL, Nikitina NI (1994) Z Metall 85:819
15. Song G, StJohn DH (2002) J Light Met 2:1
16. Zucchi F, Grassi V, Frignani A, Monticelli C, Trabanelli G (2006) J Appl Electrochem 36:195
17. Rosalbino F, Angelini E, Negri SD, Saccone A, Delfino S (2006) Intermetallics 14:1487
18. Ben-Hamu G, Eliezer D, Shin KS, Cohen S (2007) J Alloy Comp 431:269
19. Chang JW, Guo XW, Fu PH, Peng LM, Ding WJ (2007) Electrochim Acta 52:3160
20. Davis LE, MacDonald NC, Palmburg PW, Riach GE, Weber RE (1976) Handbook of AES. Perkin Elmer Corporation, Eden Prairie, MN
21. Guo XW, Chang JW, He SM, Ding WJ, Wang XS (2007) Electrochim Acta 52:2570
22. Song G, Atrens A, Dargusch M (1999) Corros Sci 41:249
23. Lunder O, Lein JE, Aune TK, Nisancioglu K (1989) Corrosion 45:741
24. Song G, Bowles AL, StJohn DH (2004) Mater Sci Eng A 366:74
25. Raman RKS (2004) Metall Mater Trans A 35:2525
26. Skar JI, Albright D, Kaplan HI (2002) Magnesium technology. The Institute of Metals, London
27. Nordlien JH, Nisancioglu K, Ono S, Masuko N (1997) J Electrochem Soc 144:461
28. Nordlien JH, Nisancioglu K, Ono S, Masuko N (1996) J Electrochem Soc 143:2564
29. Baliga CB, Tsakipoulos P (1993) Mater Sci Technol 9:513
30. Miller PL, Shaw BA, Wendt RG, Mosgier WC (1995) Corros Sci 51:922
31. Krishnamurthy S, Khobaib M, Robertson E, Froes FH (1988) Mater Sci Eng 99:507
32. Yao HB, Li Y, Wee ATS, Pan JS, Chai JW (2001) Appl Surf Sci 173:54
33. Nakatsugawa I, Kamado S, Kojima Y, Ninomiya R, Kubota K (1998) Corros Rev 16:139
34. Hara N, Kobayashi Y, Kagaya D, Akao N (2007) Corros Sci 49:166